



Optical and photovoltaic properties of new quinoxalin-2(1H)-one-based D-A organic dyes for efficient dye-sensitized solar cell using DFT

A. El Assyry^{1*}, R. Jdaa¹, B. Benali¹, M. Addou¹, A. Zarrouk²

¹Laboratoire d'Optoélectronique et de Physico-chimie des Matériaux (Unité associée au CNRST),
Université Ibn Tofail, Faculté des Sciences, B.P. 133, Kénitra, Maroc

²LCAE-URAC 18, Faculty of Science, First Mohammed University, PO Box 717, 60 000 Oujda, Morocco.

Received 06 Aug 2015, Revised 17 Sept 2015, Accepted 18 Sept 2015

*Corresponding Author. E-mail: abdeslam_elassyry@yahoo.fr; Tel: +2120662662468

Abstract

B3LYP/6-311G(d,p) quantum calculations are performed to optimize geometries and obtain properties depending on the electronic and photovoltaic for some quinoxalinone derivatives. Novel twelve organic donor- π -acceptor dyes (D- π -A), used for dye-sensitized solar cells (DSSC), based on quinoxalin-2(1H)-one were studied by density functional theory (DFT) and time dependant DFT (TDDFT) approaches to shed light on how the π -conjugation order influence the performance of the dyes. The electron acceptor group was 2-cyanoacrylic for all dyes whereas the electron-donor unit varied and the influence was investigated. The theoretical results have shown that TDDFT calculations using the Coulomb attenuating method CAM-B3LYP with the polarized split-valence 6-311G(d,p) basis sets and the polarizable continuum model (PCM) were reasonably capable of predicting the excitation energies, the absorption and the emission spectra of the molecules. The HOMO and LUMO energy levels of these dyes can ensure a positive effect on the process of electron injection and dye regeneration. The trend of the calculated HOMO-LUMO gaps nicely compares with the spectral data. Key parameters in close connection with the short-circuit current density (J_{sc}), including light-harvesting efficiency (LHE), injection driving force (ΔG^{inject}) and total reorganization energy (λ_{total}) were discussed. In addition, the estimated values of open-circuit photovoltage (V_{oc}) for these dyes were presented. The calculated results of these dyes reveal that the Q₄ dye can be used as a potential sensitizer for TiO₂ nanocrystalline solar cells due to its best electronic and optical properties and good photovoltaic parameters.

Keywords: Dye-sensitized solar cells, Quinoxalin-2(1H)-one, TDDFT, PCM, Optoelectronic, Photovoltaic parameters

1. Introduction

Considering the environmental issue and renewable resources, more and more attentions are paid to the solar energy utilizations. Dye-sensitized solar cells (DSSC) have attracted an ever-increasing attention in scientific research and in practical applications since the first report by O'Regan and Grätzel in 1991, because of its potential advantages, such as low cost and highly efficient conversion of sunlight into electricity [1-3]. In particular, these DSSC are composed of a wide band gap semi-conductor (typically TiO₂) sensitized with molecular dyes, able to capture light in the visible region of the spectrum, and a redox electrolyte (typically Iodide/triiodide I/I₃) [4-6]. In DSSC, incoming light causes electronic excitations of the dye sensitizers leading to electrons injection to the conduction band of nanocrystalline metal oxide. Then, the dyes regain electrons from redox couple in electrolyte solution [1]. In general, a power conversion efficiency dye sensitizer has the following characteristics: the highest occupied molecular orbital (HOMO) energy must be located below the HOMO energy of electrolyte to accept the electron from a redox electrolyte pair (I/I₃), and the lowest unoccupied molecular orbital (LUMO) should have a higher energy than that of the conduction band of semi-conductor (TiO₂). The sensitive dyes play an important role for DSSC to gain the higher solar-to-electricity conversion efficiency that has been an active research subject, recently [7-9]. In this context, two different kinds

of dye sensitizers are used in DSSC device: metal organic complexes and metal-free organic dyes. The metal organic complexes (e.g. the Ruthenium dyes such as N719 and N3) [10, 11] are the most promising sensitizers for DSSC and show a record power conversion efficiency of 11% under air mass (AM) 1.5 irradiation [12]. However, due to the limited availability and environment issues of the noble-metal Ruthenium, metal-free organic dyes have been developed as alternatives. Therefore, the metal free organic dye sensitizers such as coumarin [13, 14], indoline [15], triphenylamines [16-18], perylene and fluorene [19, 20], thienopyrazine [21] have also been developed and exhibited satisfactory performance. The most extensively studied organic dyes usually adopt the donor- π spacer-acceptor (D- π -A) structural motif, which exhibit several advantages: high molar extinction coefficients, low cost of production, and an extraordinary diversity [22]. In this structure, the intramolecular charge transfer (ICT) from D to A at the photoexcitation will inject the photoelectron into the conduction band of the semi-conductor through the electron accepting group at the anchoring unit. By changing the electron donor, acceptor, and/or - π -spacer group, the HOMO and LUMO energy levels are affected [23]. The quinoxalinone is rigid, coplanar and electron-accepting fused heterocycle due to the electron-withdrawing nitrogen of imine (C=N) and giving rise to a highly extended π -electron system [24]. Recent researches showed that the quinoxalinone system is a promising candidate as a core unit for high performance semi-conductors [25]. quinoxaline-based acceptors and thiophene- and pyrrole-based donors to create alternating D-A oligomers, working towards low band gap, ambipolar materials for OFET applications [25]. Recently, the study of synthesis, structural and energetic properties of quinoxalines has been done by our group [26-33]. More recently, some quinoxaline-based polymers were synthesized for polymer solar cell applications, and power conversion efficiency (PCE) up to 6–7% was reported [34-37]. Relative to quinoxaline-based polymers, quinoxaline-based small molecules photovoltaic materials remain rare [38-41]. Recently, a theoretical study of photovoltaic properties on a series of D- π -D molecules with quinoxalinone as π -spacer and different number of donor unit as photoactive components of organic bulk heterojunction (BHJ) solar cells; was reported [41]. Despite the large body of work outlined above, to the best of our knowledge the employment of quinoxaline as photosensitizers for DSSC remains rare [42].

Nowadays, theoretical quantum calculations have been effective tools in the field of chemistry because they can be used to rationalize the properties of known chemical compounds and also predict those of unknown ones to guide observed experimental synthesis [43]. In contrast to experimental results for metal-free organic dyes, the theoretical investigations are still limited. Only few research groups have studied the electronic structures and photophysical properties of dye sensitizers [42-44], and intra molecular electron dynamic process between dyes and TiO₂ nanocrystalline [45, 46]. In this context, the quinoxalinone-based organic dyes Qi ($i=1-12$) whose chemical structures are shown in Fig.1 were synthesized according to the method described in the literature [47]. The central quinoxalinone was paired through conjugation to an heterocyclic or phenylene as donor groups and linked to substituent as acceptor/anchoring group forming D- π -A architecture.

In this work, the electronic structure and optical absorption properties of twelve dye sensitizers (Fig.1) were calculated by using DFT and TDDFT. Based upon the calculated results, we analyzed the role of different electron-donor groups in the tuning the geometries, electronic structures and optical properties. Also, we aimed to see the sensitizer donor effects on the open circuit photovoltage (V_{oc}) and the short-circuit current density (J_{sc}) of the cell through discussing the key factors affecting V_{oc} and J_{sc} with the goal of finding potential sensitizers for use in DSSC.

2. Theoretical methodology

Theoretical background

The power conversion efficiency (η) is mainly determined by the short-circuit current density (J_{sc}) and the open circuit photovoltage (V_{oc}). The η can be expressed by the following equation [48]:

$$\eta = FF \frac{V_{oc} J_{sc}}{P_{inc}} \quad (1)$$

Where FF is the fill factor and P_{inc} is the incident solar power on the cell. From this expression, J_{sc} , V_{oc} , and FF are only obtained by the experiment. The relationship among these values and electronic structures for the dyes is still unknown. Herein, we aimed to see the sensitizer donor effects on the V_{oc} and J_{sc} of the cell through discussing the key factors affecting them.

For the short-circuit current density J_{sc} in DSSC, it is determined as:

$$J_{sc} = \int_{\lambda} LHE(\lambda) \Phi_{inject} \eta_{collect} d\lambda \quad (2)$$

where $LHE(\lambda)$ is the light harvesting efficiency. Φ_{inject} is the electron injection efficiency, and $\eta_{collect}$ is the charge collection efficiency. For the same DSSC with only different dyes, it is reasonable to assume that the $\eta_{collect}$ is a constant. As a result, to shed light onto the relationship between the J_{sc} and η theoretically, we investigated the LHE , Φ_{inject} and total reorganization energy (λ_{total}). From Eq. (2), to obtain a high J_{sc} , the efficient sensitizers applied in DSSC should have a large LHE , which can be expressed as [49]:

$$LHE = 1 - 10^{-f} \quad (3)$$

where f is the oscillator strength of the dye associate to the wavelength λ_{max} in the equation. We noticed that the larger oscillating strength obtained, the higher light-harvesting efficiency will have. At the same time, a large Φ_{inject} based on Eq. (2) could also guarantee a high J_{sc} , which is related to the injection driving force ΔG^{inject} and evaluated by [49]:

$$\Delta G^{inject} = E^{dye*} + E_{CB} \quad (4)$$

where E^{dye*} is the oxidation potential energy of the dye in the excited state and E_{CB} is the reduction potential of the conduction band of TiO_2 in Eq. (4), respectively. There, we use in this work $E_{CB} = -4.0$ eV for TiO_2 [50], which is widely used in some papers [49, 51, 52], and the E^{dye*} can be estimated [51-53] by:

$$E^{dye*} = E^{dye} - E_{00} \quad (5)$$

where E^{dye} is the oxidation potential energy of the dye in the ground state, while E_{00} is an electronic vertical transition energy corresponding to the λ_{max} . It is generally accepted that there are two schemes to evaluate the ΔG^{inject} , that is relaxed and unrelaxed paths. The previous works concluded that the calculation with the unrelax path is reliable [48, 52, 53]. Thus, the electron injection from excited state of dye to the TiO_2 (CB) is determined by the unrelax path in our investigation.

Additionally, as mentioned in Eq. (2), the small total reorganization energy (λ_{total}) which contains the hole and electron reorganization energy could enhance the J_{sc} . Namely, the smaller λ_{total} value obtained, the faster charge-carrier transport rates will be [49]. So we computed the hole and the electron reorganization energy (λ_h and λ_e) according to the following formula [54]:

$$\lambda_i = (E_0^{\pm} - E_{\pm}^{\pm}) + (E_{\pm}^0 - E_0) \quad (6)$$

where E_0^{\pm} is the energy of the cation or anion calculated with the optimized structure of the neutral molecule, E_{\pm}^{\pm} is the energy of the cation or anion calculated with the optimized cation or anion structure, E_{\pm}^0 is the energy of the neutral molecule calculated at the cationic or anionic state, and the E_0 is the energy of the neutral molecule at ground state.

To analyze the relationship between V_{oc} (Open-circuit photovoltage) and the energy of LUMO (E_{LUMO}) of the dyes based on electron injection from LUMO to the conduction band (E_{CB}) of the semi-conductor TiO_2 the V_{oc} (in eV) can be approximately estimated by the analytical relationship [53]:

$$V_{oc} = E_{LUMO} - E_{CB} \quad (7)$$

Computational methods

All the calculations were performed with the Gaussian 09 packages [55]. The density functional theory (DFT) with Becke's three parameter functional and the Lee–Yang–Parr functional (B3LYP) [56-58] and 6-311G(d,p) basis set was employed to investigate the structure optimization of the ground state of the dyes in gas phase. Frequency calculations were performed at the same level of theory as geometry optimization to confirm that all the optimized geometries are located at the lowest point of the potential energy surface. In a recent work, Tretiak and Magyar [59] have demonstrated for a series of D- π -A systems that a good description of the charge transfer states can be achieved when a large fraction of HF exchange is used. A newly designed functional, the long rang Coulomb attenuating method (CAM-B3LYP) considered long-range interactions by comprising 19% of HF and 81% of B88 exchange at short-range and 65% of HF plus 35% of B88 at long-range [60]. Furthermore, The CAM-B3LYP has been applied and was reasonably capable of predicting the excitation energies and the absorption spectra of the D- π -A molecules [61-62]. Therefore, the vertical excitation energy and electronic absorption spectra were simulated using TD-CAM-B3LYP method in this work. The inclusion of the solvent effect in theoretical calculations is important when seeking to reproduce or predict the experimental spectra with a reasonable accuracy. The iodure/iodide couple is used as regenerator in DSSC implying that the solar cells work in solvent phase. Polarizable continuum model (PCM) [63] has emerged in the last two decades as the most effective tool to treat bulk solvent effects for both the ground and excited-states. In this paper, the integral equation formalism polarizable continuum model (IEF-PCM) [64, 65] was chosen in excitation energy calculations. The cationic and anionic states of dyes were optimized at the B3LYP/6-311G(d,p) level to calculate the total reorganization energies (λ_{total}).

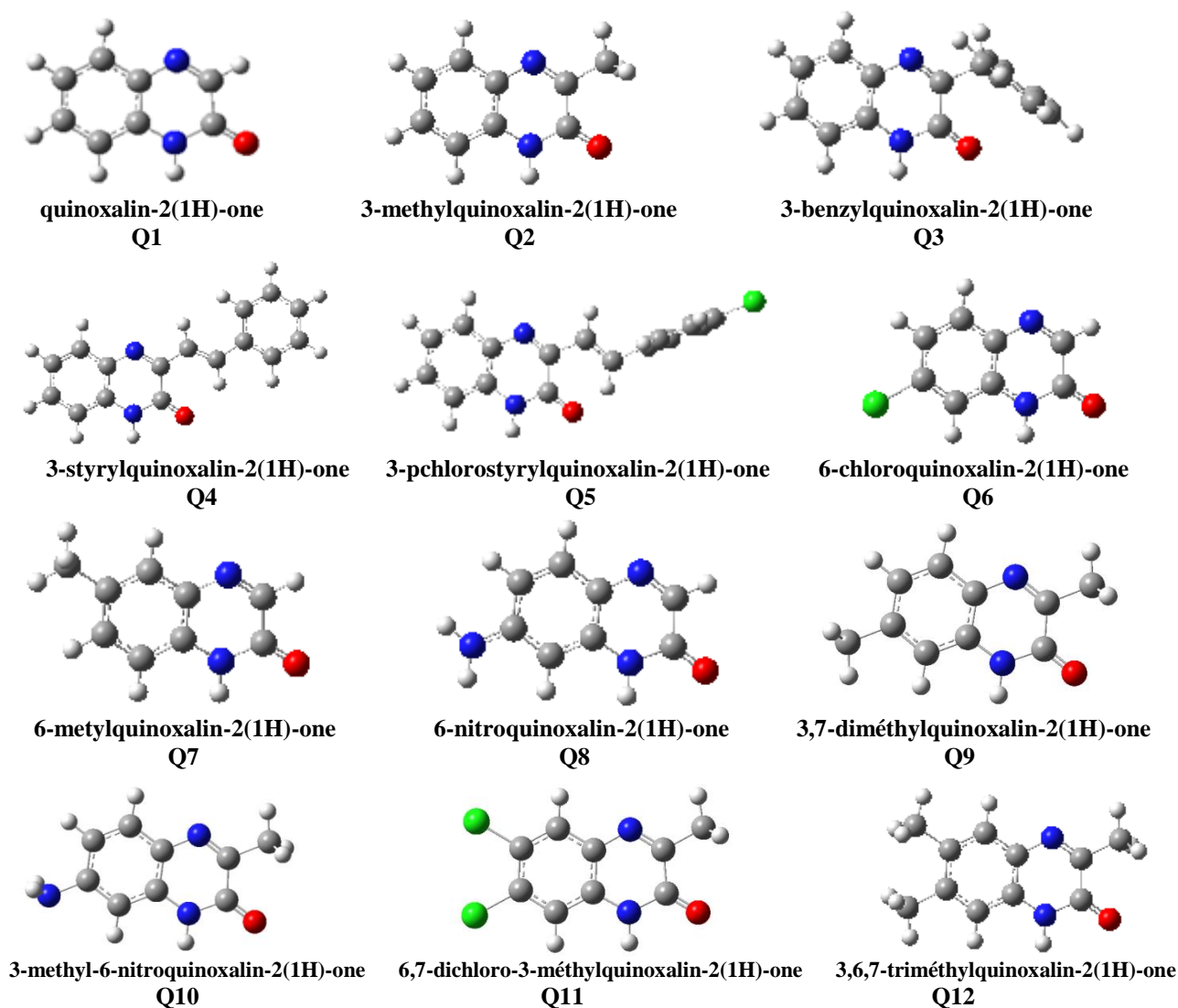


Fig. 1. Optimized geometries of all dyes.

3. Results and discussion

Molecular design and geometry structures

The chemical structures of the quinoxalinone dyes used in this work are depicted in Fig. 1. All the molecular geometries have been calculated with the B3LYP/6-311G(d,p) level. It was found in other works that the DFT-optimized geometries were in excellent agreement with the data obtained from X-ray analysis [66-68]. The optimized structures for all organic dyes (Fig. 1) show that they have similar coplanar conformation. We believe that this coplanar molecular-structure should improve the electron transfer from the electron-donor to the electron acceptor through the π -spacer unit for these dyes. For each model, the calculated critical bond lengths d_1 , d_2 and d'_1 of Q_i ($i = 1-12$) in all the ground state (S_0) and the excited state (S_1) are compared in Table 1. These corresponding geometrical parameters in S_0 are very similar with each other. This indicates that both the introduction of substituent and the elongating of the conjugate chain have little effect on these geometric parameters since the dyes have similar π -conjugated linker. We note a slight decrease of the corresponding bond distances going from (Q1, Q2, Q3) to the other dyes, which is probably due to the extension of conjugation. Moreover, the linkage between the electron-donor and π -conjugated bridge is in the range of 1.084–1.540 Å showing especially more C=C character which favors ICT. Indeed, in this D- π -A system, the p-conjugated group is employed as the bridge of ICT from the electron-donor to electron-acceptor group. On the other hand, upon photoexcitation to the excited state (S_1), the bond lengths for these dyes significantly decreased in comparison with those in the ground state (S_0), especially the linkage between the π -conjugated group and the acceptor moiety (d_2). These results indicate that the connection of acceptor group and the π -bridge (quinoxalinone) is crucial for highly enhanced ICT character, which is important for the absorption spectra red-shift.

Intramolecular charge transfer

In DSSC, one of the most important features of metal-free organic sensitizers is the intramolecular charge transfer (ICT) from donor to acceptor/anchoring group. The ICT behavior was obtained from the frontier molecular orbital (FMO) contribution [69, 70]. Herein, we plotted the electron spatial distribution of HOMO and LUMO orbitals of all dyes (Fig. 2). In general, the plots of the HOMO and LUMO demonstrated the typical π -type molecular orbital characteristics. Moreover, the HOMO displays an anti-bonding character between two adjacent fragments and bonding character within each unit. The LUMOs exhibit the bonding character between the two adjacent fragments, so the lowest lying singlet states are corresponding to electronic transition of π - π^* type [71, 72]. As observed in Fig. 2, the pattern of the HOMOs and LUMOs are qualitatively similar with each other, respectively. Moreover, the electron distributions of HOMOs are mainly located in the electron donor to the π -conjugated spacer, while the LUMOs are essentially localized on the conjugation spacer moiety and the electron acceptor fragments. Therefore, the electronic transitions of all D- π -A dyes from HOMO to LUMO could lead to ICT from the donor units to the acceptor/anchoring groups through the conjugated bridge, so that the HOMO-LUMO transition can be classified as a π - π^* ICT. The anchoring group (C=O) of all dyes has considerable contribution to the LUMOs which could lead to a strong electronic coupling with TiO₂ surface and thus improve the electron injection efficiency, and subsequently enhance the short-circuit current density J_{sc} .

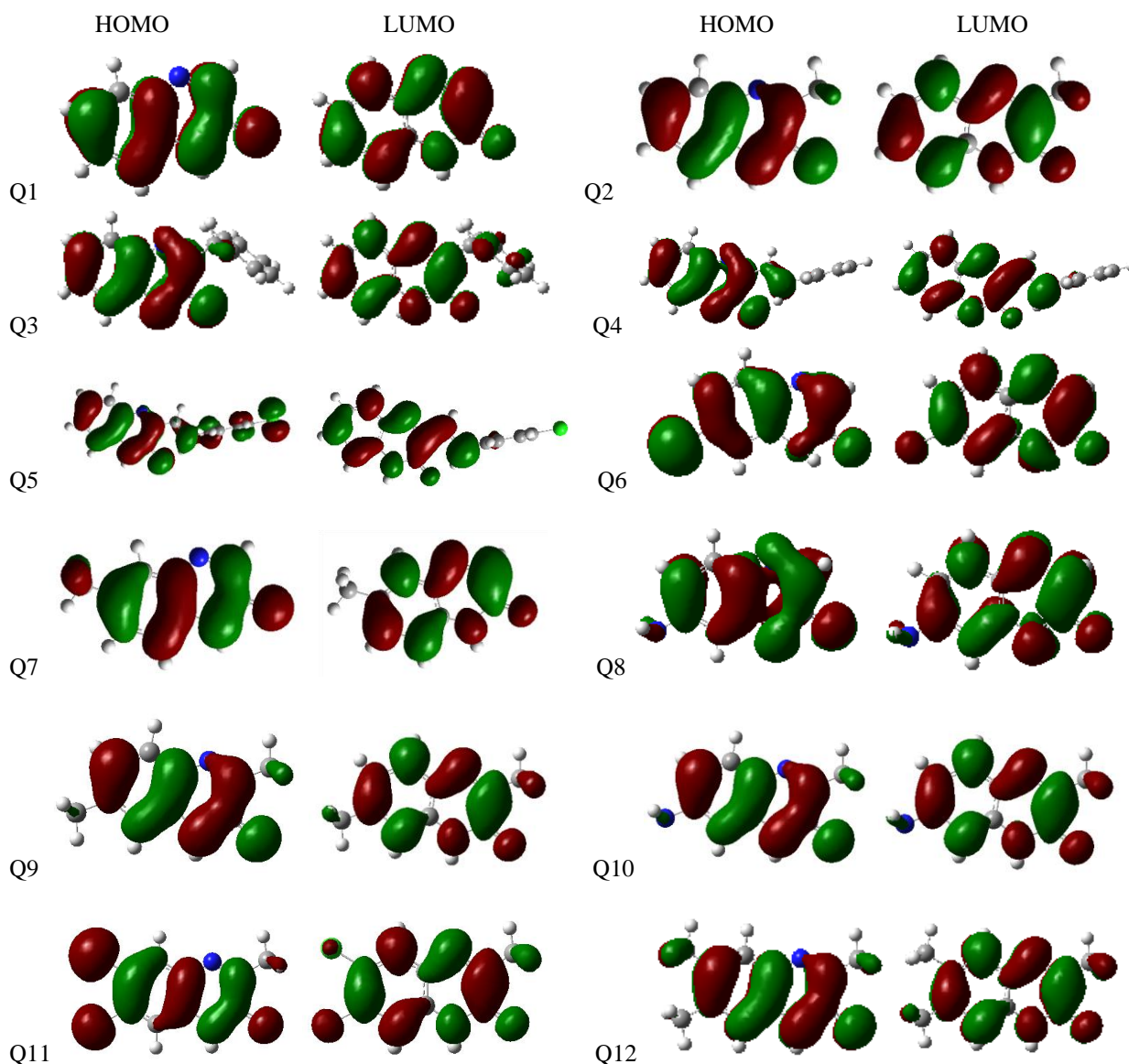


Fig. 2. Contour plots of the frontier orbitals of all dyes.

Table 1. Selected bond lengths (Å) parameters of all dyes in the ground (S_0) and excited (S_1) states.

Dye	d_1		d_2		d_3	
	S_0	S_1	S_0	S_1	S_0	S_1
Q1	1.0846	1.0823	1.0824	1.0802	1.0834	1.0815
Q2	1.5400	1.5263	1.0700	1.0672	1.0700	1.0681
Q3	1.5400	1.5247	1.0700	1.0687	1.0700	1.0679
Q4	1.4509	1.4726	1.0827	1.0762	1.0833	1.0671
Q5	1.5400	1.5236	1.0699	1.0652	1.0699	1.0661
Q6	1.0844	1.0823	1.0801	1.0768	1.8266	1.8117
Q7	1.0846	1.0817	1.5400	1.5254	1.0834	1.0816
Q8	1.0846	1.0815	1.0700	1.0674	1.4700	1.4534
Q9	1.5399	1.5248	1.0700	1.0683	1.5400	1.5252
Q10	1.5399	1.5254	1.0700	1.0678	1.4700	1.4669
Q11	1.5399	1.5257	1.7600	1.7435	1.7600	1.7435
Q12	1.5399	1.5257	1.5400	1.5260	1.5400	1.5260

Molecular orbitals

To afford deeper insight about the dependence of the electronic properties on the molecular structure, the analysis of the energy levels of the frontier molecular orbitals (HOMO and LUMO) and the related energy gap (E_g) of these dyes, is provided in Fig. 3. The electron-donating ability of the electron-donor in D- π -A dyes has the tendency to influence the electrochemical properties. A D- π -A dye with a stronger electron-donating group should give a high HOMO as compared to that with a weaker electron-donor. We have investigated the electron-donor effect on the electronic properties by using different donor groups. According to the analysis of HOMO, the results of these dyes are in order: Q11>Q8>Q4>Q6>Q12>Q7>Q2>Q9>Q10>Q1>Q3>Q5. The Q11 contains the strongest electron-donor group (dichloride) since it has the highest HOMO (-8.2179 eV). Dyes Q3 and Q5 with calculated HOMO energy levels -8.8437, -8.8437 eV, respectively, have a weak contribution in electron-donor ability due to the fact that they contain a benzene ring in the electron-donor moiety. As followed from Fig. 3, the calculated LUMO level for all sensitizers are relatively unaffected by the changes in molecular structure, due to the inclusion of same electron acceptor group (C=O) in these sensitizers, which is less influenced by the change of the donor group. The LUMO energy levels of all dyes are much higher than that of TiO₂ conduction band edge (ca. -4.0 eV) [50]. Moreover, molecules in excited states have a strong ability to inject electrons into TiO₂ electrodes. The HOMO of all dyes is lower than that of I/I_3 (ca. -4.8 eV) [73], therefore, these molecules that lose electrons could be restored by getting electrons from electrolyte. Thus, electron injection of excited molecules and, subsequently, regeneration the oxidized species is energetically permitted. This allows the application of the dyes in DSSC.

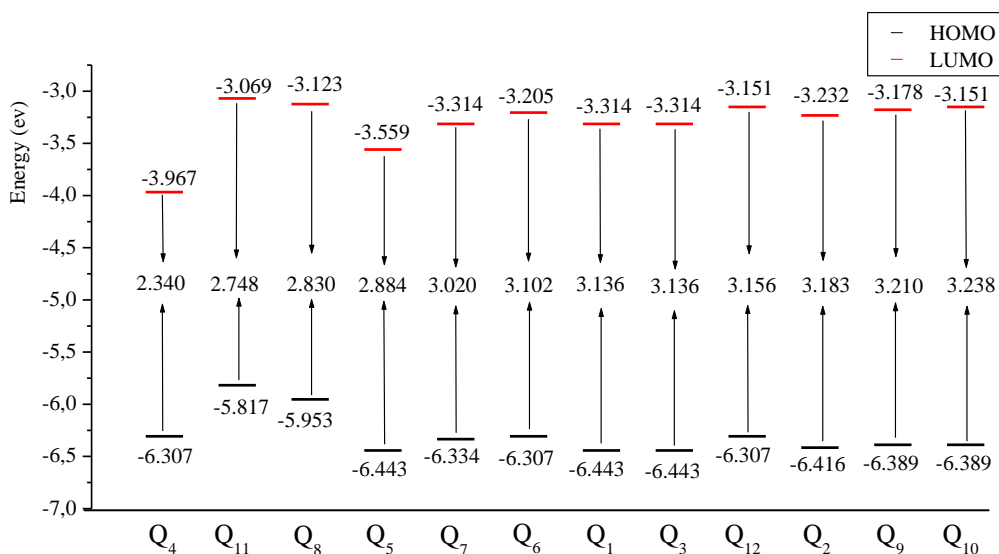


Fig. 3. Schematic energy diagram of all dyes.

The energy gap for Q_i ($i = 1-12$) was obtained by the differences of HOMO and LUMO energy levels using B3LYP/6-311G(d,p) and the results are listed in Fig. 3. The order of the E_g is: $Q_4 < Q_{11} < Q_8 < Q_5 < Q_7 < Q_6 < Q_1 < Q_3 < Q_{12} < Q_2 < Q_9 < Q_{10}$. With the HOMO–LUMO gap decrease, more photons at the longer-wavelength side would be absorbed to excite the electrons into the unoccupied molecular orbital, which increases the short-circuit current density and further enhances the conversion efficiency of the corresponding solar cell. The ranges of E_g are about 2.34–3.24 eV; we may conclude that these dyes have the potential to be employed in the DSSC application. It is found that increasing more in Q8, Q11 and Q5 gradually decreased the E_g to around 0.39, 0.44 and 0.35 eV compared to Q9, Q2 and Q10 respectively. For dyes with long conjugation length Q8–Q6, it was shown clearly that inserting the benzene and chlorine unit in the dyes Q3 and Q6 increase the E_g comparing to Q8–Q7 which contain heteroatom ring in the electron-donor group.

Optical properties

To gain insight of the optical property and electronic transition, the excitation energy and UV-Vis absorption spectra for the singlet–singlet transition of all sensitized dyes were simulated using TDDFT with CAM-B3LYP functional in chloroform solution [74, 75]. Based on the previous works, the chloroform was used as solvent in the UV-Vis absorption spectra on the quinoxaline based molecules [25, 37, 40]. The computed vertical excited singlet states, transitions energies and oscillator strength of all sensitized dyes in solvent media are tabulated in Table 2. The simulated absorption spectra of the studied compounds obtained at the IEF-PCM/TD-CAM-B3LYP/6-311G(d,p) level is shown in Fig. 4. The spectra show similar profile for all dyes; they present a main intense band at higher energies from 435 to 515 nm. The most intense contribution to the main band is an excitation from the HOMO to LUMO orbital in solvent as the first singlet excitation. As showing in Table 2, the effects of the solvent on the excitation energies of all titled compounds were found stabilized by 0.2 eV as mean averaged error, while small red-shift (~ 28 nm) was observed on the maximal wavelength (λ_{max}). Similar effects were detected on the oscillator strength (~ 0.18). On the other hand, the position (related to the gap between HOMO and LUMO levels) and the width of the first band in the spectrum are the two first parameters that can be related to the dye efficiency, since the absorption shift to lower energies favors the light harvesting process. Herein, the first vertical excitation energies (E_{ve}) of the dyes are in decreasing order: $Q_{10} > Q_9 > Q_2 > Q_{12} > Q_3 > Q_1 > Q_6 > Q_7 > Q_5 > Q_8 > Q_{11} > Q_4$ showing that there is a bathochromic shift when passing from Q10 to Q4. Compared with Q2, the absorption spectra of Q9 and Q10 show slight blue-shift with less decreased oscillator strength, due probably to the electronegativity of the heteroatom in the electron donor groups. The absorption spectra of Q3, Q4 and Q5 present the main peak at 503.17, 574.91 and 553.95 nm, respectively (Table 2), which are clearly shifted to longer wavelengths relative to those of the corresponding derivatives Q1–Q2 due to the extended π -conjugation. Moreover, the main peak of Q8, Q9, Q10 and Q11 appears red-shifted in the spectrum compared with the corresponding Q1, Q7 and Q2 by increasing the methyl unit. The absorption maxima of Q6 and Q12 are found at shorter wavelength than those of Q3–Q5 due to the lower HOMO level of benzene ring. All results of absorption spectra are in good agreement with the energy levels and band gap discussed above.

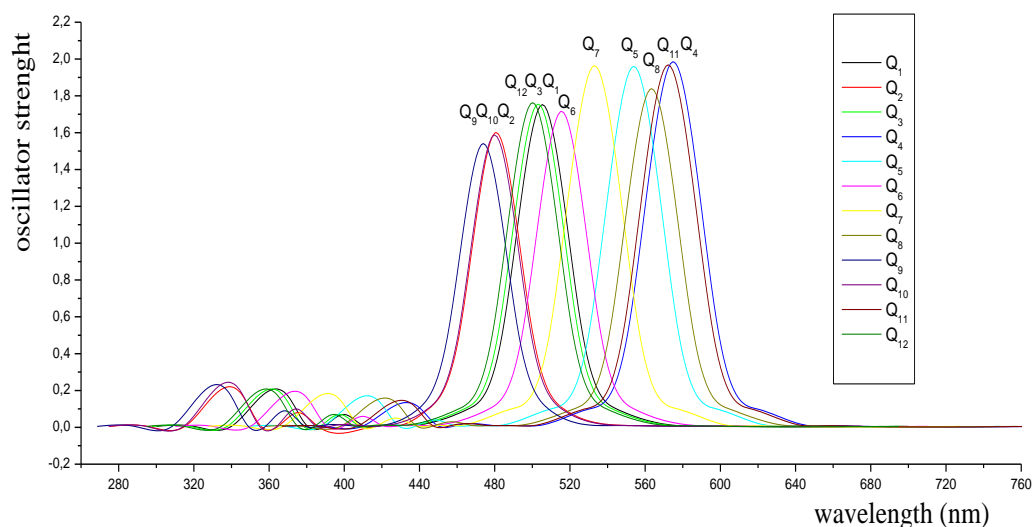


Fig. 4. Simulated absorption spectra of all dyes.

In order to study the emission photoluminescence properties of the studied compounds Q_i ($i=1-12$), the adiabatic emission spectra were obtained using the optimized geometry of the first excited singlet state at the TDDFT/CAM-B3LYP/6-311G(d,p) level. The simulated fluorescence wavelengths with the strongest oscillator are presented in Table 2. According to the absorption and emission data, the values of Stokes shift (SS) for all dyes were obtained. The emission spectra arising from S_1 state is assigned to $\pi^* \rightarrow \pi$ and LUMO \rightarrow HOMO transition character for all molecules. Through analyzing the transition configuration of the fluorescence, we found that the calculated fluorescence is just the reverse process of the lowest lying absorption. Moreover, the observed redshifted emission of the photoluminescence (PL) spectra in order: $Q_9 < Q_{10} < Q_2 < Q_{12} < Q_3 < Q_1 < Q_6 < Q_7 < Q_5 < Q_8 < Q_{11} < Q_4$ when passing from Q_9 to Q_4 is in reasonable agreement with the obtained results of absorption. Furthermore, the Stokes shift of these dyes is found to be in the range 58.8 and 105.5 nm. The Q_4 emitted at higher wavelength (574.91 nm) with strongest intensity ($f = 1.985$), and was also characterized by larger Stokes shift (105.5 nm, Table 2). These encouraging optical properties suggest that Q_4 with styryl electron-donor will be the best candidate in the DSSC devices.

Table 2. Emission spectra data for all dyes obtained with PCM-CAM-B3LYP/6-311G(d,p).

Dye	E_{00} (eV)	E_{ve} (eV)	E_{HOMO} (eV)	E_{LUMO} (eV)	ΔE (eV)	λ_{max} (nm)	f	SS (nm)	E_T (eV)	μ (Debye)
Q1	3.19	2.70	-6.443	-3.314	3.136	505.36	1.752	84.3	-13346.63	3.8922
Q2	3.23	2.84	-6.416	-3.232	3.183	480.73	1.601	64.1	-14410.89	3.1594
Q3	3.20	2.71	-6.443	-3.314	3.136	503.17	1.755	83.2	-20663.49	3.4040
Q4	2.89	2.40	-6.307	-3.967	2.340	574.91	1.985	105.5	-21694.51	2.4341
Q5	3.00	2.48	-6.443	-3.559	2.884	553.95	1.960	103.0	-34140.03	6.4885
Q6	3.17	2.66	-6.307	-3.205	3.102	515.54	1.716	90.3	-25792.91	1.4646
Q7	3.11	2.57	-6.334	-3.314	3.020	533.07	1.964	100.1	-14410.70	4.2558
Q8	2.91	2.44	-5.953	-3.123	2.830	563.40	1.839	96.9	-14844.70	7.0044
Q9	3.24	2.85	-6.389	-3.178	3.210	473.92	1.541	58.8	-15474.94	3.7563
Q10	3.32	2.88	-6.389	-3.151	3.238	479.96	1.587	76.3	-15908.43	3.6954
Q11	2.90	2.41	-5.817	-3.069	2.748	572.23	1.968	104.9	-39303.24	1.1978
Q12	3.21	2.72	-6.307	-3.151	3.156	500.15	1.763	81.6	-16484.54	4.1417

To confirm this result, we determined the dipole moment vectors in a three-dimensional representation of the quinoxalin-2(1H)-one and its eleven derivatives (fig. 5). Dipole moment μ vectors computed at the RHF/STO-3G level displayed in figure 4 lend further support to this image; μ Vectors are referred to the standard orientation of every molecule, i.e. the nuclear charge center for the molecule is at the origin of coordinates.

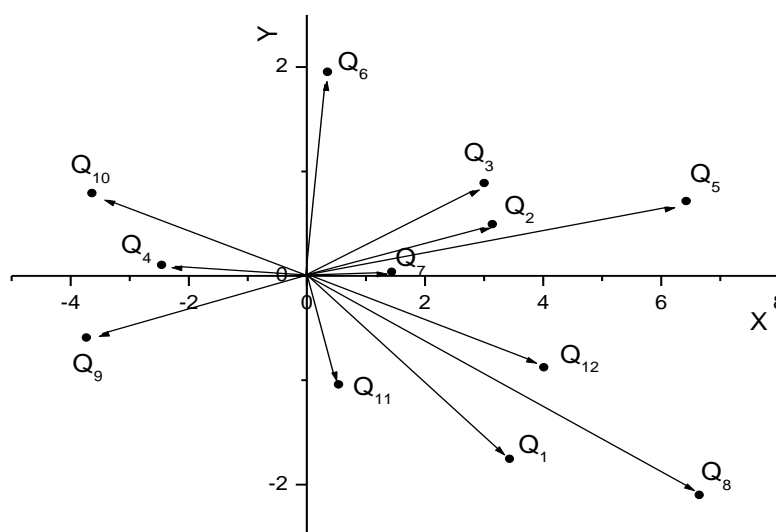


Fig. 5. Dipole moments μ (Debye) in a three-dimensional representation, computed at the RHF/STO-3G level of theory for quinoxalin-2(1H)-one derivatives in Fig. 1.

The dipole moment for Q1 (3.892 D) is increased when more pchlorostyryl and nitro are added away from position 3 and 7 in Q5 (6.488 D) and Q8 (7.004 D) with an orientation (+54° and +13°) and decreased when they are replaced in Q7, Q2 and Q3 with an weak orientation, and even effect at summer noted in the compound Q11 and Q12 with a small orientation (~12°). However, the variations of μ in these seven cases is considerably smaller than that found in Q6, Q9, Q10 and Q4 where the presence of electronegative chlorine in the opposite side with respect to carbonyl not only reduces dramatically the dipole moment but also changes the vector orientation with large angle (-140° in Q4) (Fig. 5). The information provided by NPA charges as well as this change with regard to μ are in agreement with the known weak resonance effect of chlorine, already known [76-78], as compared with its inductive effect.

Photovoltaic properties

The electronic injection free energy ΔG^{inject} , ground E^{dye} and excited E^{dye^*} state oxidation potentials computed for the dyes Q_i are represented in Table 3. Based on Koopman's theorem, ground state oxidation potential energy is related to ionization potential energy.

E^{dye} can be estimated as negative E_{HOMO} [79]. E^{dye^*} is calculated based on Eq. (5). E^{dye^*} of all dyes is increasing order: Q4<Q11<Q12<Q3=Q8<Q1<Q9<Q2=Q6<Q5<Q7<Q10. It shows that the most convenient oxidizing species is Q4 while Q10 is the worst. All ΔG^{inject} estimated from Eq. (4) is in negative value for all sensitizers, thus the electron injection from the dye to TiO_2 is spontaneous.

As seen from Table 3 and Fig. 6(a) the calculated ΔG^{inject} are decreased in the order: Q4>Q11>Q12>Q3=Q8>Q1>Q9>Q2=Q6>Q5>Q7>Q10. It shows that Q4 has the largest ΔG^{inject} value while Q10 has the smallest. Another factor related to efficiency of DSSC is the performance of the dyes responsible of the incident light. Based on the LHE of the dyes, the value has to be as high as possible to maximize the photocurrent response. The LHE values for all dyes are in narrow range 0.971–0.989 (Table 3), but increase slightly with increasing the conjugation length (Fig. 6(b)). This means that all the sensitizers give similar photocurrent.

Table 3. Estimated electrochemical parameters for all dyes.

Dye	E^{dye} (eV)	E^{dye^*} (eV)	ΔG^{inject} (eV)	LHE	λ_h (eV)	λ_e (eV)	λ_{total} (eV)	V_{oc} (eV)
Q1	6.26	3.07	-0.93	0.982	0.282	0.321	0.603	0.686
Q2	6.36	3.13	-0.87	0.974	0.273	0.317	0.590	0.768
Q3	6.24	3.04	-0.96	0.982	0.280	0.332	0.612	0.686
Q4	5.84	2.95	-1.05	0.989	0.213	0.281	0.494	0.033
Q5	6.15	3.15	-0.85	0.989	0.240	0.302	0.542	0.441
Q6	6.30	3.13	-0.87	0.980	0.231	0.313	0.544	0.795
Q7	6.38	3.27	-0.73	0.989	0.270	0.300	0.570	0.686
Q8	5.95	3.04	-0.96	0.985	0.241	0.272	0.513	0.877
Q9	6.32	3.08	-0.92	0.971	0.263	0.321	0.584	0.822
Q10	6.61	3.29	-0.71	0.974	0.280	0.352	0.632	0.849
Q11	5.88	2.98	-1.02	0.989	0.221	0.280	0.501	0.931
Q12	6.20	2.99	-1.01	0.982	0.293	0.332	0.625	0.849

As we know, besides the reaction free energy, the reorganization energy λ_{total} could also affect the kinetics of electron injection. So, the calculated λ_{total} is also important to analyze the relationship between the electronic structure and the J_{sc} . As mentioned in section 'Theoretical background', the small λ_{total} which contains the hole and electron reorganization energy could enhance the J_{sc} . As seen from Table 3 and Fig. 6(c) the calculated λ_{total} of all dyes are increased in the order: Q4<Q11<Q8<Q5< Q6<Q7<Q9<Q2<Q1<Q3<Q12<Q10. It shows that dye Q4 possesses the smallest total reorganization energy while dye Q10 has the largest. As a result, dye Q4 exhibits a favorable J_{sc} due to the relative similar LHE, larger ΔG^{inject} and smaller λ_{total} . At the same time, ΔG^{inject} and λ_{total} are more important to govern the J_{sc} mostly. We know that besides the short-circuit current density J_{sc} the overall power conversion efficiency η also could be influenced by the open-circuit voltage (V_{oc}). Therefore, between two dyes with similar structures, the electron injection would be more efficient for that dye with the higher excited state related to the semi-conductor conduction band edge (i.e. higher V_{oc}). Based on Eq. (7), it was found that V_{oc} of all dyes (Table 3) is in the range 1.469–2.367 eV and in decreasing order: Q4>Q5>Q1=Q3=Q7>Q2>Q6>Q9>Q10=Q12>Q8>Q11. It shows that Q4 and Q5 have the larger V_{oc} values than other dyes, while Q8 and Q11 have the smallest. As a consequence of the above data, we could draw a conclusion that the large LHE, ΔG^{inject} , V_{oc} as well as small λ_{total} could have a high efficiency. Thus, the

performance of DSSC sensitized by dye Q4 might be superior to the other dyes, due to its favorable performances of the above factors based on our computed results.

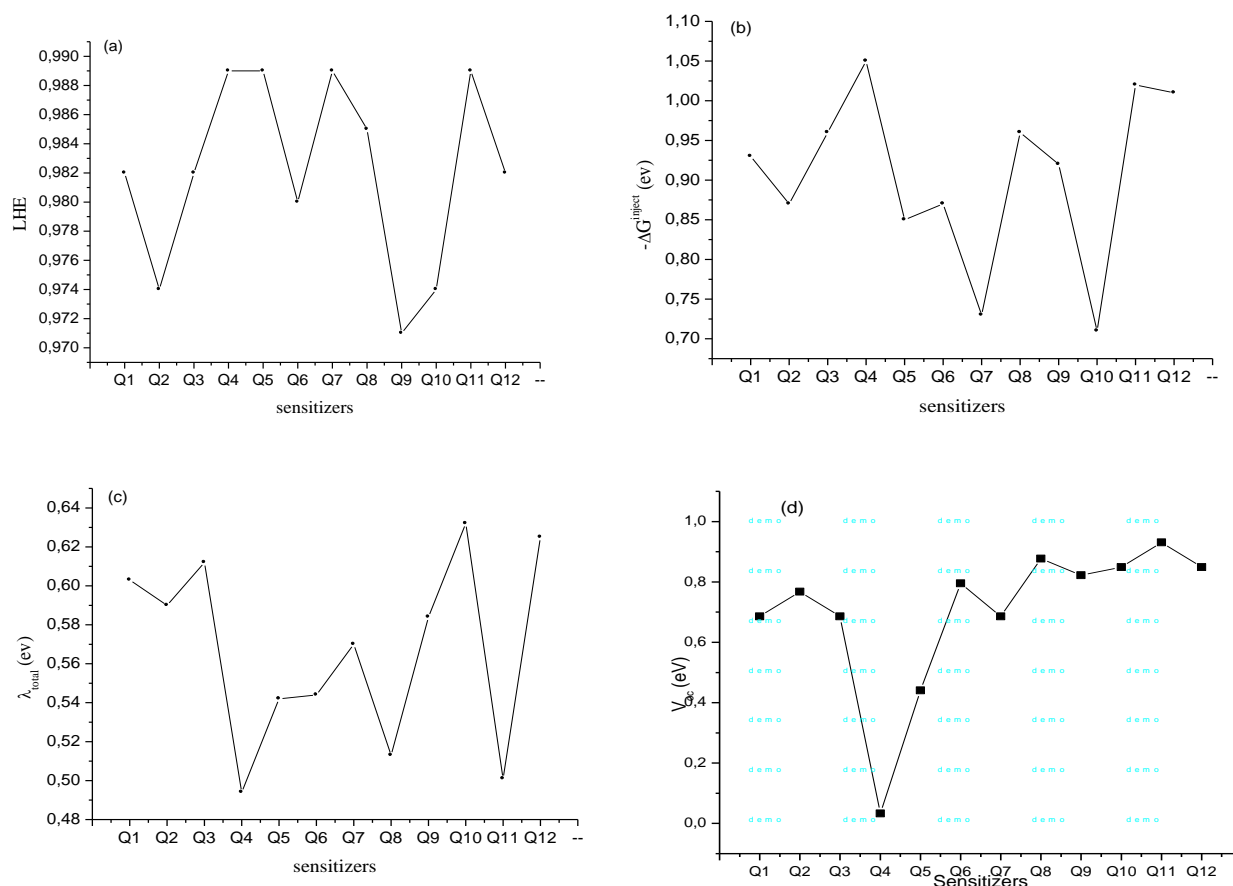


Fig. 6. Critical parameters influenced J_{sc} along of investigated sensitizers: (a) the light-harvesting efficiency, (b) the electronic injection free energy, (c) the reorganization energy λ_{total} and (d) the open-circuit voltage V_{oc} .

Conclusion

In this study, the electronic structure and optical absorption properties of twelve selected quinoxalin-2(1H)-one dye sensitizers were investigated by using DFT and TDDFT. Based upon on the calculated results, we have analyzed the role of different electron-donor groups in the tuning the geometries, electronic structures and optical properties. Also, we have aimed to see the sensitizer donor effects on the V_{oc} and J_{sc} of the cell through discussing the key factors affecting V_{oc} and J_{sc} with the goal of finding potential sensitizers for use in DSSC. It can be concluded that this class of selected quinoxalin-2(1H)-one dyes shows a good photophysical properties related to DSSC use but in different outstanding properties. The Q4 dye possessing styryl donor group was found to be the best photosensitizer for use in DSSC, with respect to the other dyes, as the calculation results show its good oxidation potential energy and electron injection force that lie over the E_{CB} of TiO_2 and under reduction potential energy of the electrolyte. This theoretical approach presents a guiding tool to the synthesis process and helps to understand the structure-properties relationship of these new systems.

Acknowledgments-This work has been supported by the Hassan II Academy of Science and Technology. The authors are grateful to Professor Mohamed Addou (Dean of the Faculty of Science and Technology in Tangier-Morocco) for the explication of solar cell applications.

References

1. Grätzel M., *Nature.*, 414 (2001) 338-344.
2. Hagfeldt A., Grätzel M., *Acc. Chem. Res.*, 33 (2000) 269-277.
3. O'Regan B., Grätzel M., *Nature.*, 353 (1991) 737-740.
4. Kamat P.V., Haria M., Hotchandani S., *J. Phys. Chem. B*, 108 (2004) 5166-5170.

5. Bisquert J., Cahen D., Hodes G., Ruehle S., Zaban A., *J. Phys. Chem. B*, 108 (2004) 8106-8118.
6. Furube A., Katoh R., Yoshihara T., Hara K., Murata S., Arakawa H., Tachiya M., *J. Phys. Chem. B*, 108 (2004) 12583-12592.
7. Tian Z., Huang M., Zhao B., Huang H., Feng X., Nie Y., Shen P., Tan S., *Dyes Pigm*, 87 (2010) 181-187.
8. Matsui M., Ito A., Kotani M., Kubota Y., Funabiki K., Jin J., Yoshida T., Minoura H., Miura H., *Dyes Pigm*, 80 (2009) 233-238.
9. Ma X., Wu W., Zhang Q., Guo F., Meng F., Hua J., *Dyes Pigm*. 82 (2009) 353-359.
10. Nazeeruddin M.K., Kay A., Rodicio I., Humphry-Baker R., Mueller E., Liska P., Vlachopoulos N., Gratzel M., *J. Am. Chem. Soc.* 115 (1993) 6382-6390.
11. Nazeeruddin M.K., Zakeeruddin S.M., Humphry-Baker R., Jirousek M., Liska P., Vlachopoulos N., Shklover V., Fischer C.H., Gratzel M., *Inorg. Chem.*, 38 (1999) 6298-6305.
12. Nogueira A.F., Longo C., De Paoli M.A., *Coord. Chem. Rev.* 248 (2004) 1455-1468.
13. Wang S.Z., Cui Y., Hara K., Dan-Oh Y., Kasada C., Shinpo A., *Adv. Mater.* 19 (2007) 1138-1141.
14. Wong B.M., Codaro J.G., *J. Chem. Phys.* 129 (2008) 214703-214711.
15. Horiuchi T., Miura H., Sumioka K., Uchid S., *J. Am. Chem. Soc.* 126 (2004) 12218-12219.
16. Chunyang J., Zhongquan W., Jiaqiang Z., Zi L., Xiaojun Y., Yu S., *Spectrochim. Acta, Part A*, 86 (2012) 387.
17. Zeng W.D., Cao Y.M., Bai Y., Wang Y.H., Shi Y.S., Wang P., *Chem. Mater.*, 22 (2010) 1915-1925.
18. Li G., Zhou Y., Cao X., Bao P., Jiang K., Lin Y., *Chem. Commun.*, 16 (2009) 2201-2203.
19. Ferrere S., Zaban A., *J. Phys. Chem. B*, 101 (1997) 4490-4493.
20. Ferrere S., Gregg B., *New J. Chem.*, 26 (2002) 1155-1160.
21. Bourass M., Touimi Benjelloun A., Hamidi M., Benzakour M., Mcharfi M., Sfaira M., Serein-Spirauc F., Lère-Portec J.P., Sotiropoulos J.M., Bouachrine M., *J. Saudi. Chem. Soc.*, DOI:10.1016/j.jscs.2013.01.003.
22. Casanova D., *Chem. Phys. Chem.*, 12 (2011) 2979-2988.
23. Xu J., Wang L., Liang G., Bai Z., Wang L., Xu W., Shen X., *Spectrochim. Acta, Part A*, 78 (2011) 287-293.
24. Lin Y., Fan H., Li Y., Zhan X., *Adv. Mater.*, 24 (2012) 3087-3106.
25. Dong Wook Chang, Seo-Jin Ko, Jin Young Kim, Liming Dai, Jong-Beom Baek, *Synth. Met.*, 162 (2012) 1169.
26. El Assyry A., Benali B., Lakhrissi B., El Faydy M., Ebn Touhami M., Touir R., Touil M., *Res. Chem. Intermed.*, 41 (2015) 3419-3431.
27. Ben Hmamou D., Salghi R., Zarrouk A., Zarrok H., Hammouti B., Al-Deyab S. S., El Assyry A., Benchat N., Bouachrine M., *Int. J. Electrochem. Sci.*, 8 (2013) 11526-11545.
28. Benhiba F., ELaoufir Y., Belayachi M., Zarrok H., El Assyry A., Zarrouk A., Hammouti B., Ebnou E. E., Guenbour A., Al Deyab S. S. and Oudda H., *Der Pharm. Lett.*, 6 (2014) 306-318.
29. Larouj M., ELaoufir Y., Serrar H., El Assyry A., Galai M., Zarrouk A., Hammouti B., Guenbour A., El Midaoui A., Boukhriss S., Ebn Touhami M. and Oudda H., *Der Pharm. Lett.*, 6 (2014) 324-334.
30. El Assyry A., Benali B., Boucetta A., Lakhrissi B., *J. Struct. Chem.*, 55 (2014) 38-44.
31. Tayebi H., Bourazmi H., Himmi B., El Assyry A., Ramli Y., Zarrouk A., Geunbour A., Hammouti B., *Der Pharm. Chem.*, 6 (2014) 220-234.
32. Benali B., Lazar Z., Boucetta A., El Assyry A., Lakhrissi B., Massoui M., Jermoumi C., P. Negrier, J. M. Leger, Mondieig D., *Spectrosc. Lett.*, 41 (2008) 64-71.
33. El Assyry A., Benali B., Jdaa R., Lakhrissi B., Touil M., Zarrouk A., *J. Mater. Environ. Sci.*, 5 (2014) 1434.
34. Qiang Peng, Xiangju Liu, Yuancheng Qin, Jun Xu, Mingjun Liaand, Liming Dai, *J. Mater. Chem.*, 21 (2011) 7714-7722.
35. Hsieh-Chih Chen, Ying-Hsiao Chen, Chung-Hao Liu, Yen-Hao Hsu, Yun-Chen Chien, Wei-Ti Chuang, Chih-Yang Cheng, Chien-Liang Liu, Shang-Wei Chou, Shih-Huang Tung, Pi-Tai Chou, *Polym.Chem.*, 4 (2013) 3411-3418.
36. Yoonkyoo Lee, Thomas P. Russell, Won Ho Jo, *Org. Electron.*, 11 (2010) 846-853.
37. Fu Y., Cha H., Song S., Lee G.-Y., Park C. E., Park T., *J. Polym. Sci., Part A: Polym. Chem.*, 51 (2013) 372.
38. Velusamy M., Huang J.-H., Hsu Y.-C., Chou H.-H., Ho K.-C., Wu P.-L., Chang W.-H., Lin J. T., Chu C.-W., *Org. Lett.*, 11 (2009) 4898-4901.
39. Dhananjaya Kekuda, Jen-Shien Huang, Marappan Velusamy, Jiann T. Lin, Chih Wei Chu, *Sol. Energy Mater. Sol. Cells*, 94 (2010) 1767-1771.
40. Lu X., Feng Q., Lan T., Zhou G., and Wang Z. S., *Chem. Mater.*, 24 (2012) 3179-3187.
41. Chang D. W., Lee H. J., Kim J. H., Park S. Y., Park S.-M., Dai L., Baek J.-B., *Org. Lett.*, 13 (2011) 3880.

42. Dessì A., Consiglio G.B., Calamante M., Reginato G., Mordini A., Peruzzini M., Taddei M., Sinicropi A., Parisi M. L., Biani F. F., Basosi R., Mori R., Spatola M., Bruzzi M., Zani L., *Eur. J. Org. Chem.* 2013 (2013) 1916-1928.
43. Belghiti N., Bennani M., Hamidi M., Bouzzine S.M., Bouachrine M., *Afr. J. Pure. Appl. Chem.* 6 (2012) 164.
44. Zhang C.R., Liu Z.J., Chen Y.H., Chen H. S., Wu Y.Z., Yuan L.H., *J. Mol. Struct. (Theochem)*, 899 (2009) 86.
45. Duncan W.R., Prezhdo O.V., *J. Am. Chem. Soc.*, 130 (2008) 9756-9762.
46. Guo Z., Liang W.Z., Zhao Y., Chen G.H., *J. Phys. Chem. C*, 112 (2008) 16655-16662.
47. Ramli Y., Benzeid H., Bouhfid R., Kandri Rodi Y., Ferfra S., Essassi E.M., *St. Cerc. St. CICBIA*, 11 (2010) 67.
48. Narayan M.R., *Renew. Sust. Energy. Rev.* 16 (2012) 208-215.
49. Zhang Z.L., Zou L.Y., Ren A.M., Liu Y.F., Feng J.K., Sun C.C., *Dyes Pigm.* 96 (2013) 349-363.
50. Asbury J.B., Wang Y.Q., Hao E., Ghosh H., Lian T., *Res. Chem. Intermed.* 27 (2001) 393-406.
51. Zhang J., Li H.B., Sun S.L., Geng Y., Wu Y., Su Z.M., *J. Mater. Chem.* 22 (2012) 568-576.
52. Ding W.L., Wang D.M., Geng Z.Y., Zhao X.L., Xu W.B., *Dyes Pigm.* 98 (2013) 125-135.
53. Sang-aroon W., Saekow S., Amornkitbamrung V., *J. Photochem. Photobiol. A*, 236 (2012) 35-40.
54. Balanay M.P., Kim D.H., *J. Mol. Struct. (Theochem)*, 910 (2009) 20-26.
55. Frisch M.J., Trucks G.W., Schlegel H.B., Scuseria G.E., Robb M.A., Cheeseman J.R., et al., Gaussian 09, revision A.02, Gaussian, Inc., Pittsburgh, PA, 2009.
56. Becke A.D., *J. Chem. Phys.*, 98 (1993) 1372-1377.
57. El Assyry A., Benali B., Boucetta A., Lakhrissi B., *J. Mater. Environ. Sci.*, 5 (2014) 1860-1867.
58. Lee C., Yang W., Parr R.G., *Reviews B*, 37 (1988) 785-789.
59. Magyar R.J., Tretiak S., *J. Chem. Theory. Comput.* 3 (2007) 976-987.
60. Xue Y., An L., Zheng Y., Zhang L., Gong X., Qian Y., Liu Y., *Comput. Theor. Chem.*, 981 (2012) 90-99.
61. Camino B., De-La-Pierre M., Ferrari A.M., *J. Mol. Struct.* 1046 (2013) 116-123.
62. Irfan A., Jin R., Al-Sehemi A.G., Asiri A.M., *Spectrochim. Acta, Part A*, 110 (2013) 60-66.
63. Tomasi J., Mennucci B., Cammi R., *Chem. Rev.*, 105 (2005) 2999-3093.
64. Cossi M., Barone V., *J. Chem. Phys.*, 115 (2001) 4708-4717.
65. Adamo C., Barone V., *Chem. Phys. Lett.*, 330 (2000) 152-160.
66. Zhang X.H., Wang L.Y., Zhai G.H., Wen Z.Y., Zhang Z.X., *J. Mol. Struct.*, 881 (2008) 117-122.
67. Mondieig D., Negrier Ph., Leger J.M., Lakhrissi L., El Assyry A., Lakhrissi B., Essassi E.M., Benali B., Boucetta A., *Russ. J. Phys. Chem. A*, 89 (2015) 807-811.
68. Négrier Ph., Mondieig D., Léger J. M., Benali B., Lazar Z., Boucetta A., Elassyry A., Lakhrissi B., Jermoumi C., Massoui M., *Anal. Sci.*, 22 (2006) 175-176.
69. Benali B., Lazar Z., Elblidi K., Lakhrissi B., Massoui M., Elassyry A., Cazeau-Dubroca C., *J. Mol. Liq.*, 128 (2006) 42-45.
70. El assyry A., Benali B., Boucetta A., Lazar Z., Lakhrissi B., Massoui M., Mondieig D., *Spectrosc. Lett.*, 42 (2009) 203-209.
71. Benali B., El Assyry A., Boucetta A., Lazar Z., Lakhrissi B., Massoui M., Mondieig D., *Spectrosc. Lett.*, 40 (2007) 893-901.
72. Elassyry A., Benali B., Lazar Z., Elblidi K., Lakhrissi B., Massoui M., Mondieig D., *J. Mol. Liq.*, 128 (2006) 46.
73. Hagfeldt A., Grätzel M., *Chem. Rev.*, 95 (1995) 49-68.
74. Jacquemin D., Perpète E.A., Ciofini I., Adamo C., *Acc. Chem. Res.*, 42 (2009) 326-334.
75. Adamo C., Jacquemin D., *Chem. Soc. Rev.*, 42 (2013) 845-856.
76. El Assyry A., Benali B., Boucetta A., Mondieig D., *Res. Chem. Intermed.*, 40 (2014) 1043-1052.
77. Lazar Z., Benali B., Elblidi K., Zenkouar M., Lakhrissi B., Massoui M., Kabouchi B., Cazeau-Dubroca C., *J. Mol. Liq.*, 106 (2003) 89-95.
78. El Assyry A., Benali B., *Res. Chem. Intermed.*, 40 (2014) 627-636.
79. Pearson R.G., *Inorg. Chem.*, 27 (1988) 734-740.

(2015) ; <http://www.jmaterenvirosci.com>